Reversible Hydrogen Spillover at Atomic Interface for Efficient Hydrogen Evolution

Tingting Chao, Wenbo Xie, Yanmin Hu, Tonghui Zhao, Cai Chen, Zedong Zhang, Ge Yu, Xun Hong, Huile Jin, Dingsheng Wang, Wei Chen*, Xinhua Li*, P. Hu*, Yadong Li*

Experimental Details

Chemicals.

Ammonium molybdate tetrahydrate was purchased from Innochem. Ethylenediamine and acetic acid were purchased from Sinopharm Chemical Reagent Co. Ltd (Ourchem). Ruthenium (III) chloride was purchased from Sigma-Aldrich. Commercial Pt/C (20 wt%) was obtained from Alfa Aesar. 5 wt% Nafion solution was purchased from Sigma-Aldrich. Deionized water was used throughout our experiments. All chemicals were used as received without further purification.

Fabrication of Mo_2C NSs and Ru_1-Mo_2C NSs.

First, a piece of NF with the size of 2×0.75 cm^2 was impregnated in HCl (3.0 M) solution under ultrasound for 15 min to remove the surface oxide species. The obtained NF was washed with deionized water for several times and dried at 60 ^{o}C in vacuum oven for further use. Then, the precursor was prepared via a hydrothermal method as follows. 0.48 mmol ammonium molybdate tetrahydrate and 0.88 mL ethylenediamine were uniformly dissolved into 30.0 mL of deionized water under ultrasound condition. Then appropriate amounts of acetic acid were dripped into the aforementioned solution to adjust the pH values to 4-5. Then the solution was transferred into a Teflon-lined stainless steel autoclave and the treated NF was put into it. The sealed autoclave was heated to 150 ^{o}C and maintained for 12 h. After the reaction finished, the obtained

sample was washed with deionized water and dried at 60 °C in vacuum oven. The Mo$_2$C NSs were obtained by calcinating the precursors under 5% H$_2$/N$_2$ atmosphere for 2 h with a heating rate of 5 °C/min to reach the temperature of 450 °C. The mass loading amounts of molybdenum carbide on Ni foam is 4.07 mg cm^{-2}.

To prepare Ru-Mo$_2$C NSs, 0.5 mL of RuCl$_3$ solution (10 mg/mL) was redispersed into 30 mL of deionized water and then Mo$_2$C NSs were impregnated into it at 30 °C for 24 h. Then the adsorbed Ru species was reduced at 300 °C for 2 h under 5% H$_2$/N$_2$ atmosphere to obtain Ru$_1$-Mo$_2$C NSs.

Characterization.

Transmission electron microscopy (TEM) images of all samples were recorded on a Hitachi H-7700 operated at 100 kV. The scanning electron microscopy (SEM) images of samples were acquired by Genimi SEM 500. Aberration-corrected high-angle annular dark-field scanning transmission electron microscopy (HAADF-STEM) images and the corresponding electron energy-loss spectroscopy of samples were recorded on a JEOL JEM-2010 LaB6 high-resolution transmission electron microscope and double Cs-corrected JEOL JEM-ARM200F scanning transmission electron microscopy working at 200 kV. The electron-energy loss spectroscopy (EELS) was obtained using the GATAN GIF Quantum 965 system. The exposure time was set as 0.5 s and energy resolution was estimated as 1.5 eV. Background subtraction was performed with power low function and double arctangent function. The energy-dispersive X-ray spectroscopy (EDX) of samples was conducted on JSM-6700F. Inductively coupled plasma and atomic emission spectrum (ICP-AES) was conducted on Optima 7300 DV. The X-ray diffraction (XRD) patterns of samples were collected by Rigaku Miniflex-600 operating at the voltage of 40 kV and the current 15 mA with Cu Ka radiation (I = 1.5418 Å). X-ray photoelectron spectroscopy (XPS) was conducted on Thermo ESCALAB 250 using a Al Ka (hv =1486.6 eV) radiation source. The X-ray absorption fine structure spectra data was collected at 1W1B station in Beijing Synchrotron Radiation Facility (BSRF, operated at 2.5 GeV with a maximum current of 250 mA). The data for Mo K-edge were collected at room temperature using

a transmission mode. All samples were pelletized as disks of 13 mm diameter with 1 mm thickness using graphite powder as a binder.

Electrochemical measurements.

The electrocatalytic hydrogen evolution reaction tests were equipped with the electrochemical workstation (CHI 760E) and adopted a conventional three-electrode system at room temperature. The catalysts were grown on Ni foam with peace of 2 x 0.75 cm^2 as the working electrode, Hg/HgO and graphite rod were used as the reference electrode and counter electrode, respectively. The HER performance was carried out in N_2-saturated 1 M KOH solution with a sweep rate of 5 mV s^{-1}. All potentials were corrected with iR to a reversible hydrogen electrode (RHE), where the R was referred to the resistance arising from electrolyte/contact resistance tested by electrochemical impedance spectroscopy (EIS). The frequency of EIS measurements wat set from 100 kHz to 0.01 Hz. The electrochemical durability was evaluated by 10,000 cyclic voltammetry sweeps and chronoamperometry measurement was conducted at the potential of −56.8 mV for 140 hours. The electrochemical surface area (ECSA) was evaluated by the electrochemical double layer capacitance (C_{dl}) with a potential range from 0.22-0.32 V versus RHE at different scan rates (20, 40, 60, 80, 100, 120 mV s^{-1}) in the non-Faraday zone. The TOFs for HER can be calculated with the following equation:

$$TOF = \frac{I}{2NF}$$

I represents current during the linear sweep measurement. N represents number of active sites. F is the Faraday constant (96485.3 C/mol). 2 means two electrons are required to form one hydrogen molecule.

AEMWE test.

The Ru_1/Mo_2C and commercial Pt/C (20 wt.% Pt, Alfa Aesar) were used as the cathodic catalysts, and homemade NiFe layered double hydroxide was used as the anodic catalyst. X37-50 (Dioxide Materials Sustainion®) was used as the anion

exchange membrane (AEM) and immersed in 1 M KOH solution for at least 36 h prior to being used to exchange Cl^- into OH^-. To prepare the catalyst ink, 12 mg of Ru_1-Mo_2C catalysts were homogeneously dispensed into 4 mL of mixed solvent containing ultrapure water, ethanol and Dupont D521 under sonication for about 1 h at room temperature. Cathodic electrodes were fabricated by the catalyst coated membrane (CCM) method. The well dispersed catalyst ink was then sprayed with a spray gun until the loading was ~3 mg cm^{-2} (~13 µg$_{Ru}$ cm^{-2}) for cathode. Subsequently, the catalyst-coated membrane was sandwiched with porous carbon paper (TGP-H-060, Toray) and Ni foam gas diffusion layers (GDLs) to assemble into a homemade integrated AEMWE device. Electrically insulating gaskets were also placed to prevent the liquid and gas from escaping through any space between flow fields. Note that except for the cathodic catalysts, other experimental conditions including the assembly techniques of the device and the testing parameters kept identical. The AEMWE electrolyser was operated at the temperature of 65 °C under an ambient pressure using 1 M KOH as the electrolyte. The performance of the AEMWEs with an active area of 2 cm × 2 cm was evaluated by measuring the polarization curves from 1.2 to 2.4 V. The stability of the AEMWEs was evaluated by measuring chronopotentiometry at a current density of 500 mA cm^{-2} at the temperature of 65 °C.

Calculation Methods

In this work, all the DFT calculations were carried out with the Vienna *Ab Initio* Simulation Package (VASP)[1,2] under the framework of the generalized gradient approximation (GGA) with the Perdew-Burke-Ernzerhof (PBE) functional.[3] PBE-D3 (BJ) is also included to describe van der Waals interaction.[4] The projector-augmented-wave (PAW)[2,5] pseudopotentials were used, and the cutoff energy of plane-wave basis expansion was set to 450 eV. The Mo_2C (200), Ru_1-Mo_2C (200), and Ru(0001) surfaces are modeled with p(4×4) supercells. During the DFT calculation, the k-point sampling

was carefully examined to assure that the calculation results are converged.[6] The top three layers of the metal surface were fully relaxed, while the bottom three layers were fixed. A 15 Å vacuum layer was built above all surfaces. The constructed Mo_2C (200) is shown in Figure S12. The transition states (TS) were searched using the constrained minimization technique and the quasi-Newton algorithm.[7–10] Vibrational analysis was further used to confirm the TS with only one imaginary frequency. In the calculation of electronic structures and PDOS analysis, DFT with hybrid functionals proposed by HSE06 was used. Thermodynamic corrections are applied on all adsorption and transition states using DFT calculations, based on vibrational frequencies. The standard molar Gibbs free energy can be achieved by adding the thermodynamic corrections of zero-point-energy (ZPE), thermal energy (U) and entropy (S) derived from vibrational partition function as

$$\Delta G_{ads} = E_{ads} + \Delta ZPE + \Delta U - T\Delta S$$

Where E_{ads} is the total energies from VASP calculation. Each of the transition states was checked by the vibrational frequency analysis.

The adsorption energy of adsorbate is defined as:

$$E_{ads} = E_{R*} - E_{slab} - E_R$$

where E_{R*}, E_{slab}, and E_R represent the energies of species R adsorbed on the surface, the surface, and R in the gas phase, respectively. In the case of the adsorption energy of H atom, $0.5\ E_{H2}$ was used for the energy calculation. The more negative of E_{ads} is, the more strongly the adsorbate binds with the surface and *vice versa*.

The Ru_1-Mo_2C(200) surface model(shown in Figure S13) was built by replacing one of

the Mo atoms on the $Mo_2C(200)$ surface. The exact position of the Ru atom was determined by the formation energy of the surface. The formation energy was calculated as follows:

$$E_f = E_{total} - E_{support} - E_{Ru}$$

Where E_{total}, $E_{support}$, and E_{Ru} are the total energies of the Ru embodied Ru_1-$Mo_2C(200)$ surface, the $Mo_2C(200)$ surface, and a single Ru atom, respectively.
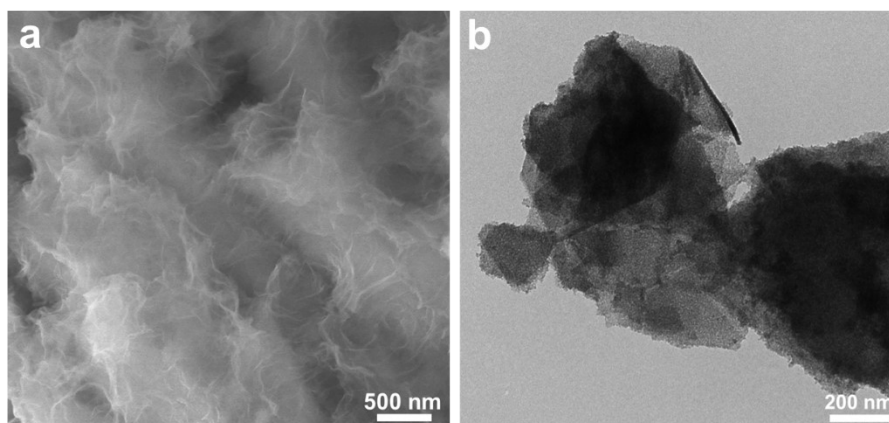
Figure S1. **Morphological and compositional characterization of Mo₂C NSs.** (a) SEM image and (b) TEM image.
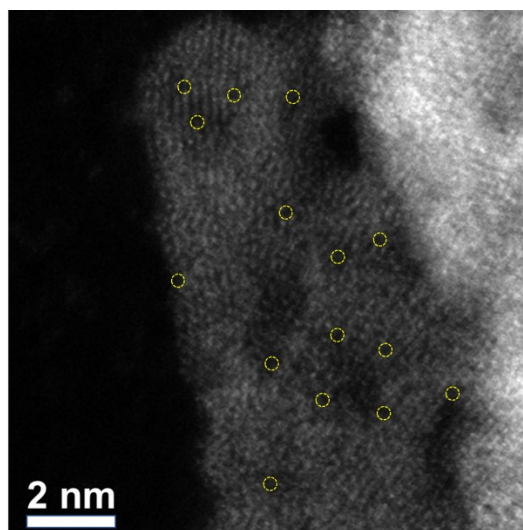
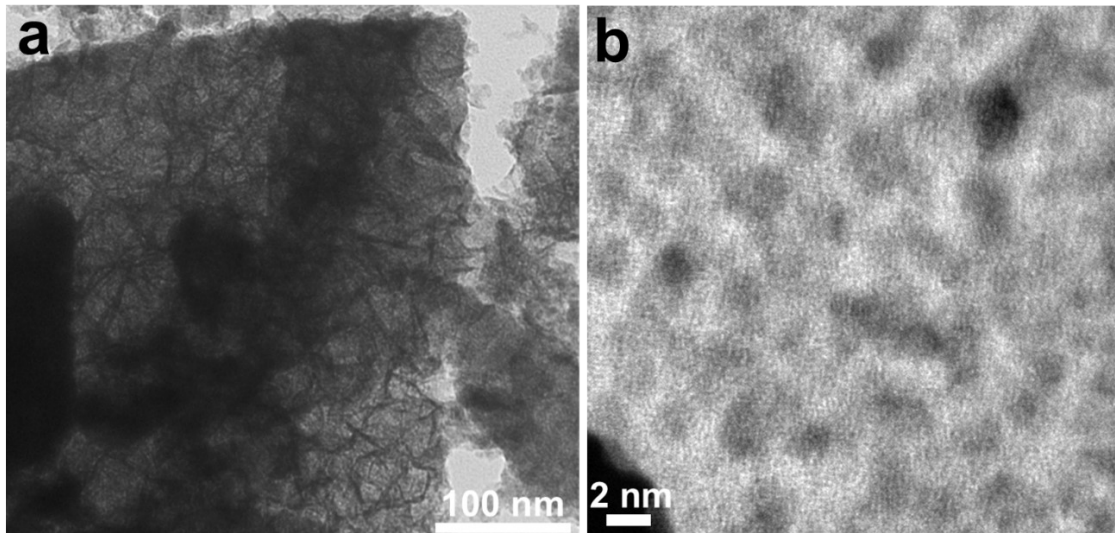**Figure S2**. HADDF-STEM image of Mo₂C NSs. Yellow circles represent the vacancy or defects.

Figure S3. (a) TEM image and (b) HADDF-STEM image of Ru_1-Mo_2C NSs.
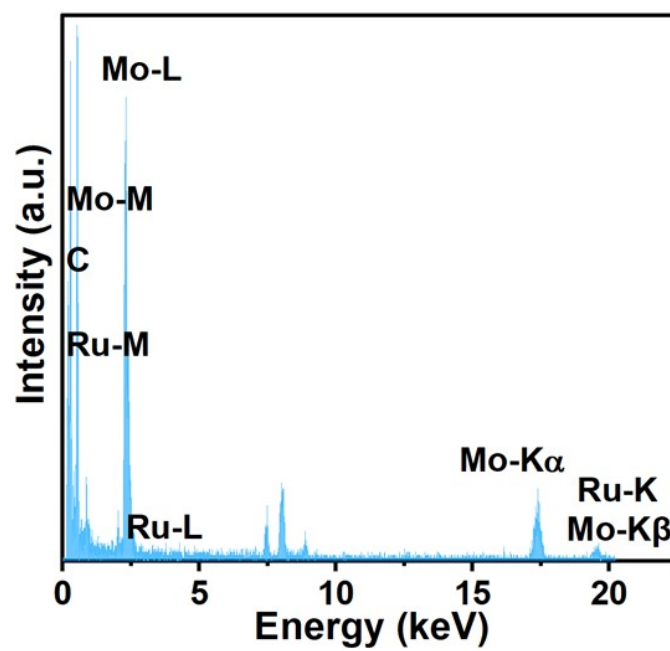

Figure S4. STEM-EDS spectrum of Ru_1-Mo_2C NSs. Inset shows the contents of Ru, Mo and C elements.
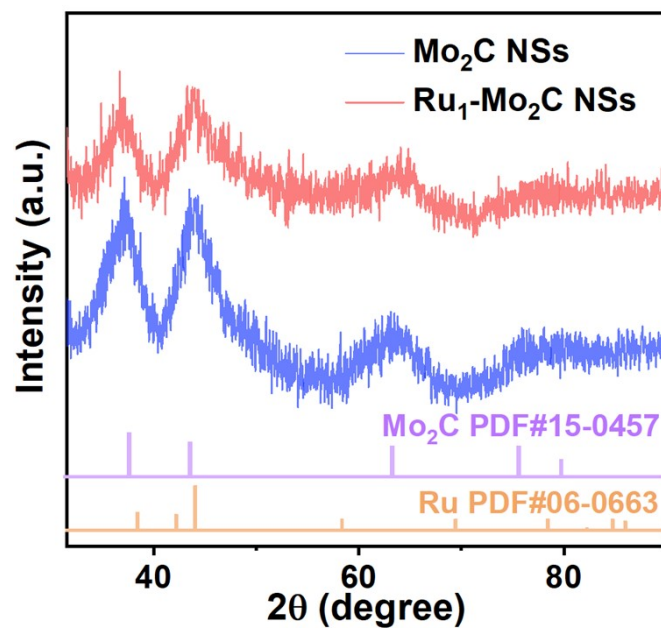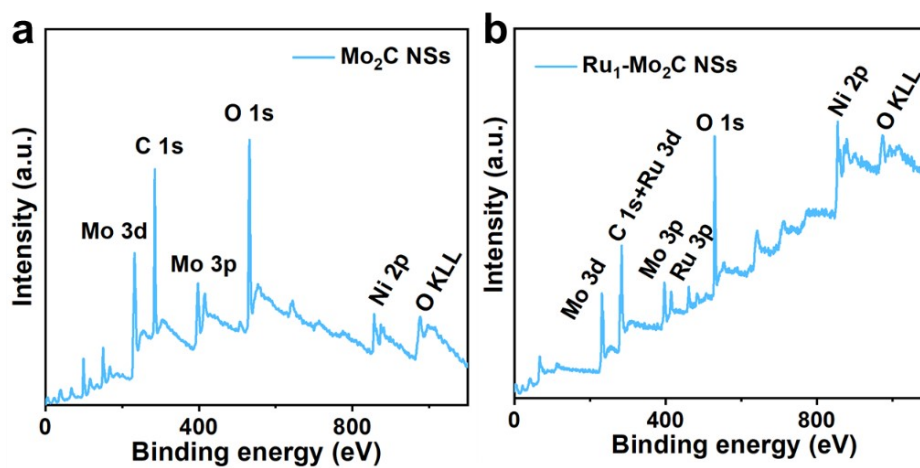
Figure S5. XRD spectra of Mo_2C NSs and Ru_1-Mo_2C NSs.

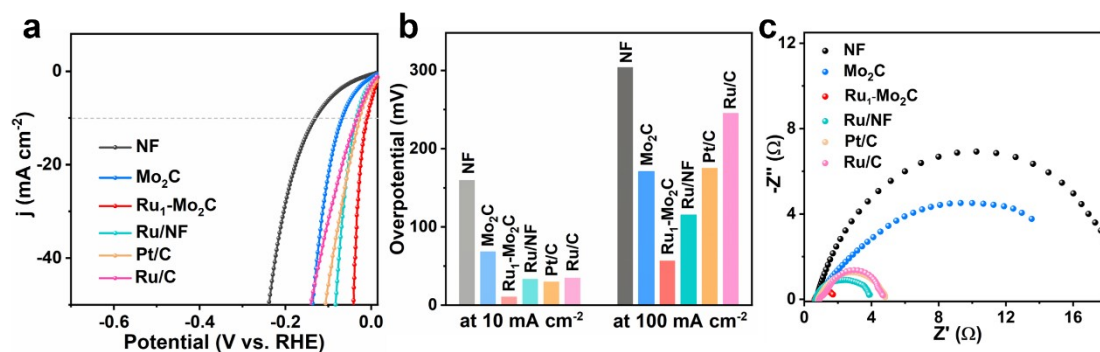**Figure S6.** XPS spectra of (a) Mo_2C NSs and (b) Ru_1-Mo_2C NSs.

Figure S7. (a) HER polarization curves of Ni foam (NF), Ru_1-Mo_2C NSs, Mo_2C NSs, Ru/NF, commercial Pt/C and Ru/C electrocatalysts in 1 M KOH electrolyte. (b) Comparison of the overpotential at the current densities of 10 mA cm^{-2} and 100 mA cm^{-2} for different catalysts. (c) Nyquist plots for iR correction.
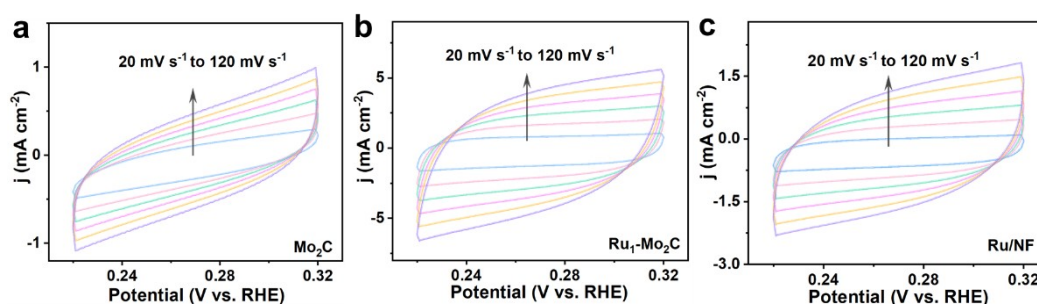

Figure S8. CV curves of (a) Mo_2C NSs, (b) Ru_1-Mo_2C NSs, and (c) Ru/NF tested with a scan rate from 20 mV s^{-1} to 120 mV s^{-1}, respectively.
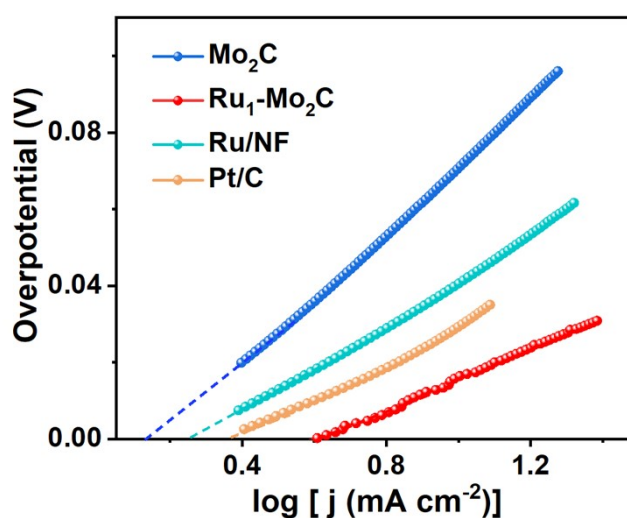

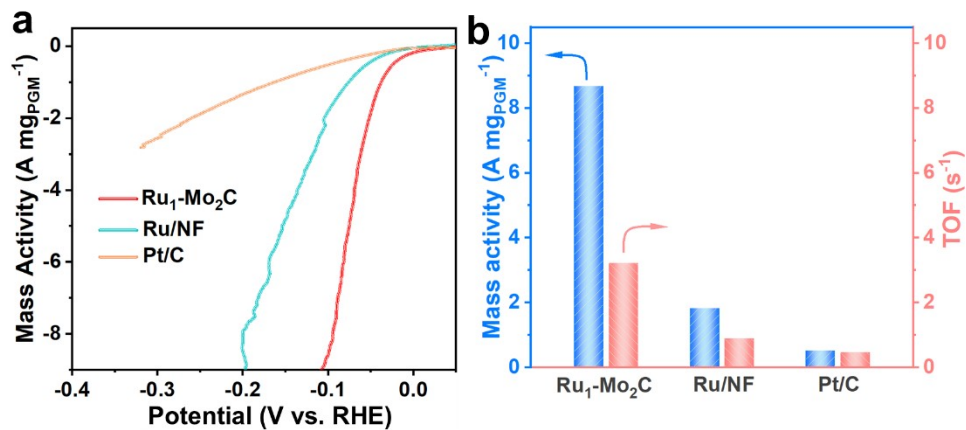**Figure S9.** Exchange current densities obtained via extrapolation method.

Figure S10. (a) LSV curves of Ru_1-Mo_2C NSs, Ru/NF and Pt/C normalized by actual mass of noble metals (Ru or Pt). (b) Mass activities (left) calculated from the mass of noble metals and TOF (right) for different catalysts.
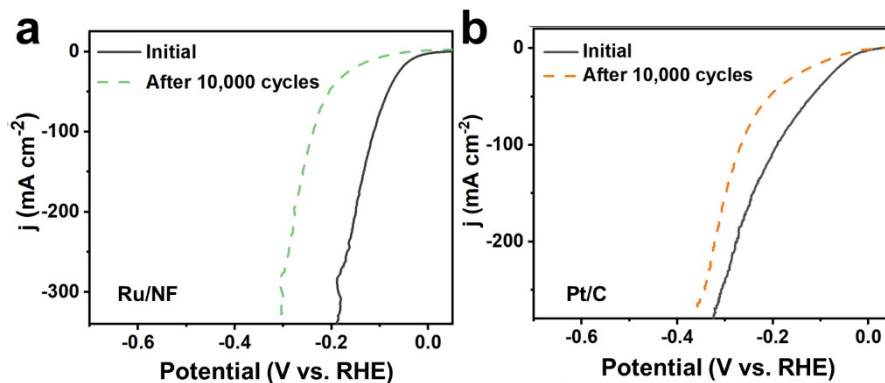
Figure S11. Polarization curves of (a) Ru/NF and (b) commercial Pt/C before and after 10,000 continuous cycles.
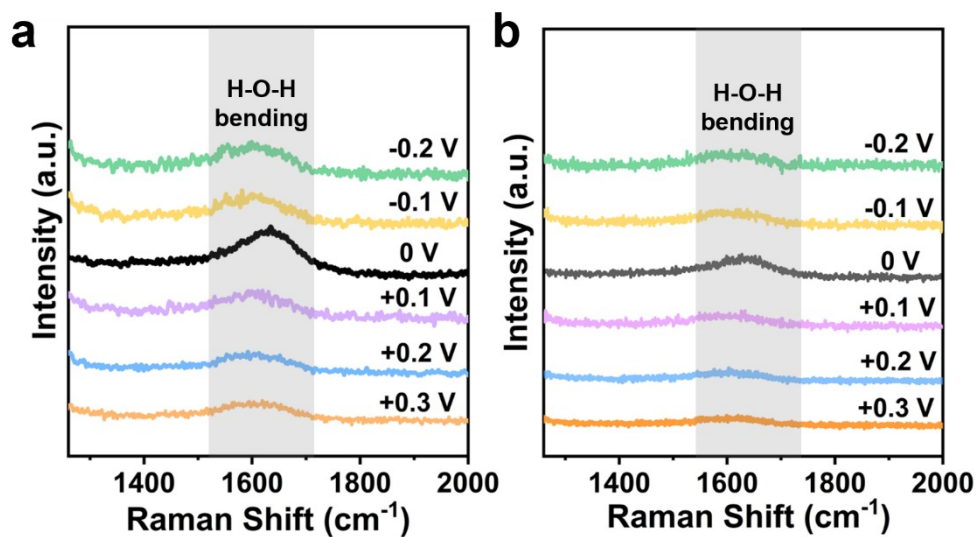
Figure S12. Operando Raman spectra of (a) Ru_1-Mo_2C and (b) Ru/NF at different

potential versus RHE in 1 M KOH electrolyte.
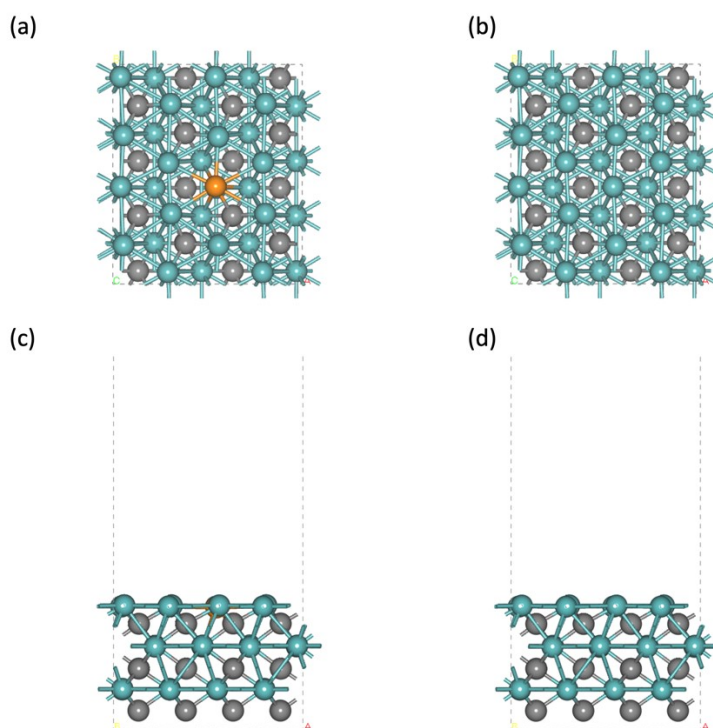
Figure S13. Top view (a) and side view (c) of the simulation surface model of Ru_1-

Mo_2C (200). Top view (b) and side view (d) of the simulation surface model of Mo_2C

(200). The Ru, Mo, and C atoms are respectively displayed in orange, cyan and grey.
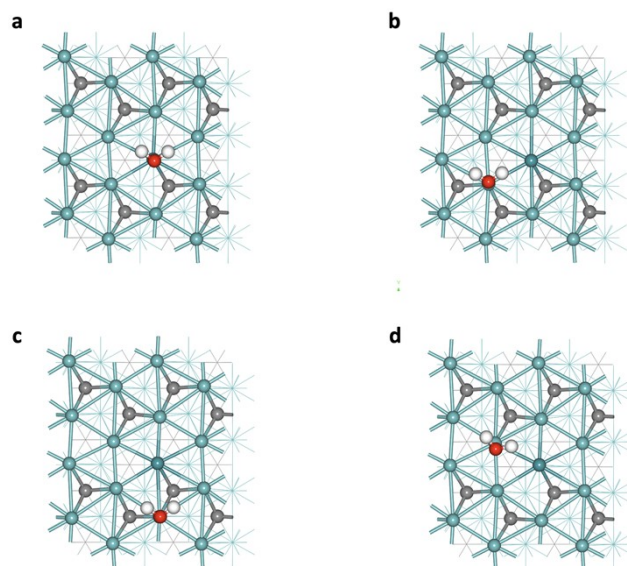
Figure S14. Adsorption structures of H_2O on different sites on Ru_1-$Mo_2C(200)$ surface.

(a) The adsorption of H_2O on the Ru single atom. (b)-(d). The adsorptions structures of

H2O on different Mo sites.
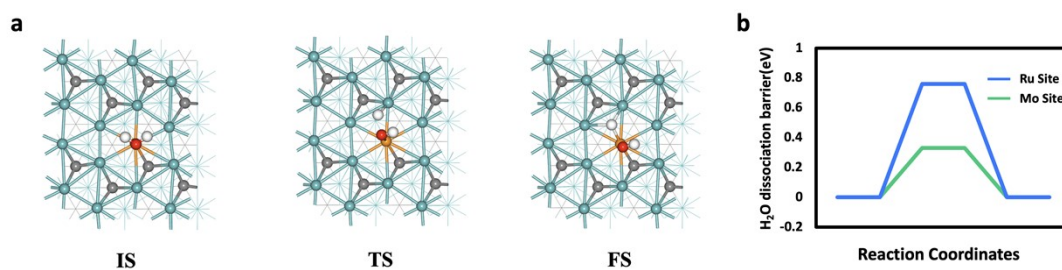
Figure S15. (a) Top view of water dissociation on the Ru site of Ru_1-$Mo_2C(200)$. The

Ru, Mo, and C atoms are displayed in orange, cyan and grey, respectively. (b)

Comparison of the reaction barriers of water dissociation on the single atom Ru site

(blue line) and the favorable Mo site (green line).
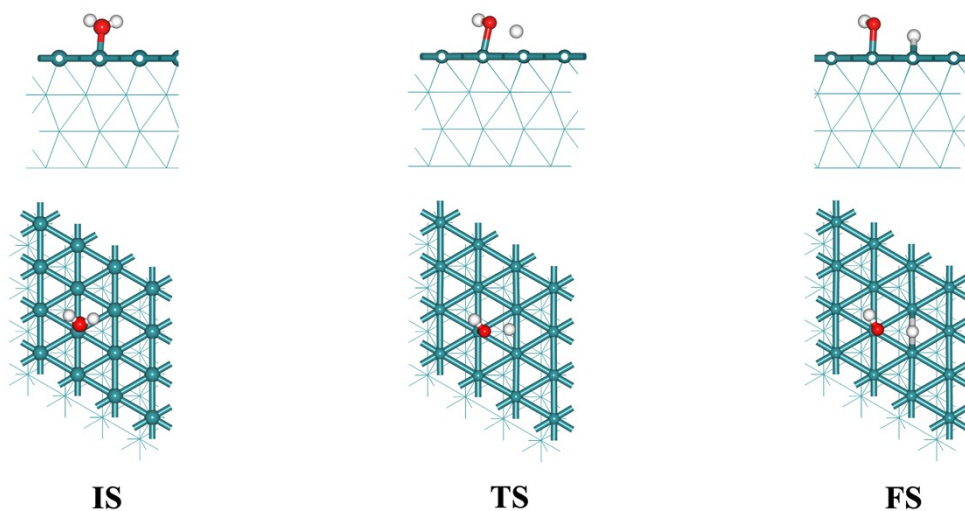
Figure S16. The mechanism of water dissociation on Ru (0001) from top and side view. The Ru, O, and H atoms are respectively displayed in cyan, red, and white.
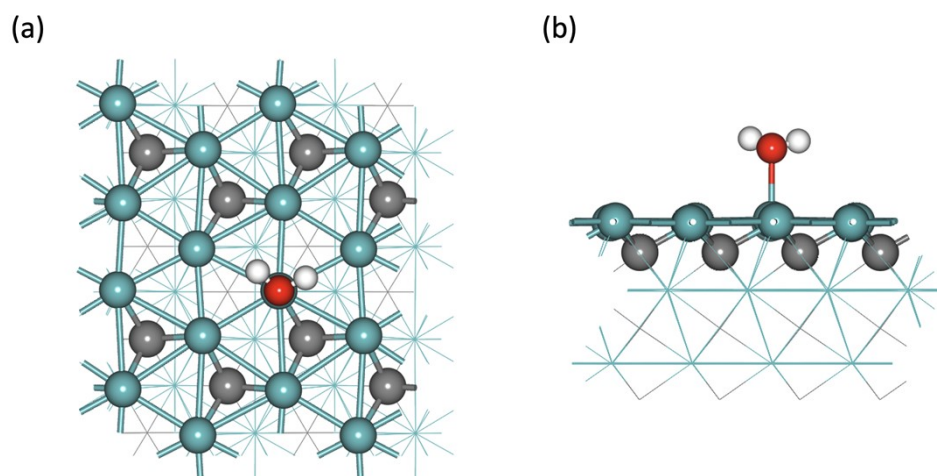
Figure S17. The adsorption structure of H_2O on the Mo at the Mo_2C (200) from (a) top and (b) side view. The Mo, C, O, H atoms are respectively displayed in cyan, dark green, grey, red and white.

IS	TS	FS
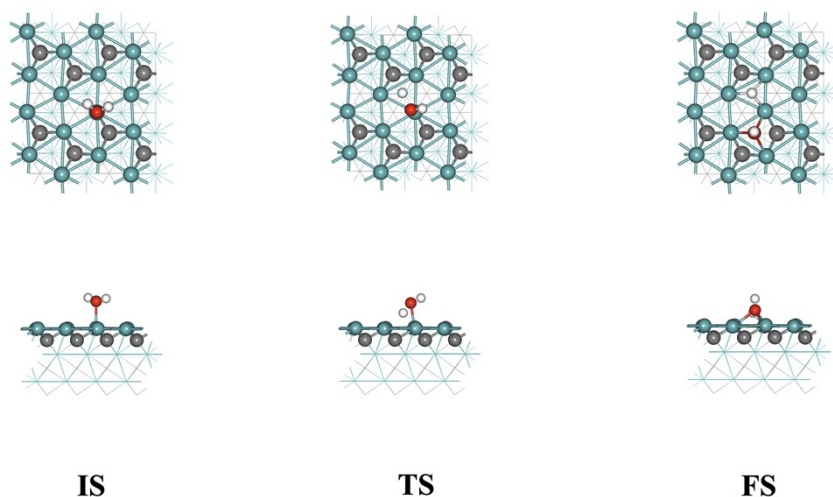
Figure S18. The mechanism of water dissociation on $Mo_2C(200)$ from top and side view. The Mo, C, O, H atoms are respectively displayed in cyan, dark green, grey, red and white.
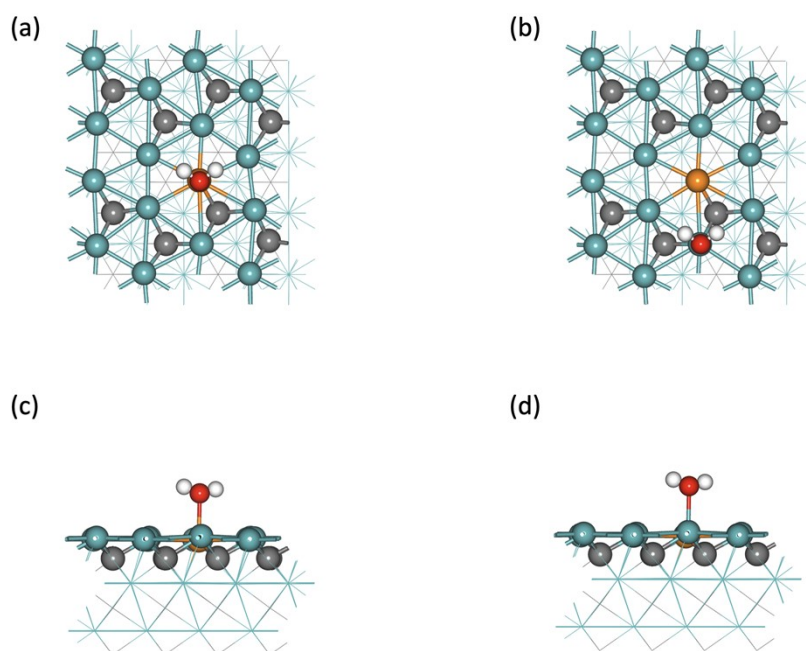
Figure S19. (a) and (c) The adsorption structure of H_2O on the Ru at the Ru_1-Mo_2C (200) from top and side view. (b) and (d) The adsorption structure of H_2O on the Mo at the Ru_1-Mo_2C (200) from top and side view. The Mo, Ru, C, H, and O atoms are respectively displayed in cyan, organ, grey, white, and red.
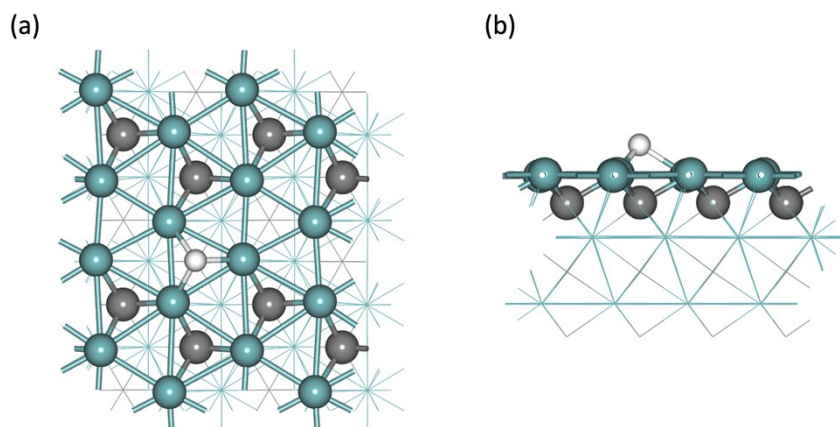
Figure S20. (a) and (b) The adsorption structure of H atom on the Mo$_2$C (200) from top and side view. The Mo, C, and H atoms are respectively displayed in cyan, grey, and white.

IS   TS   FS
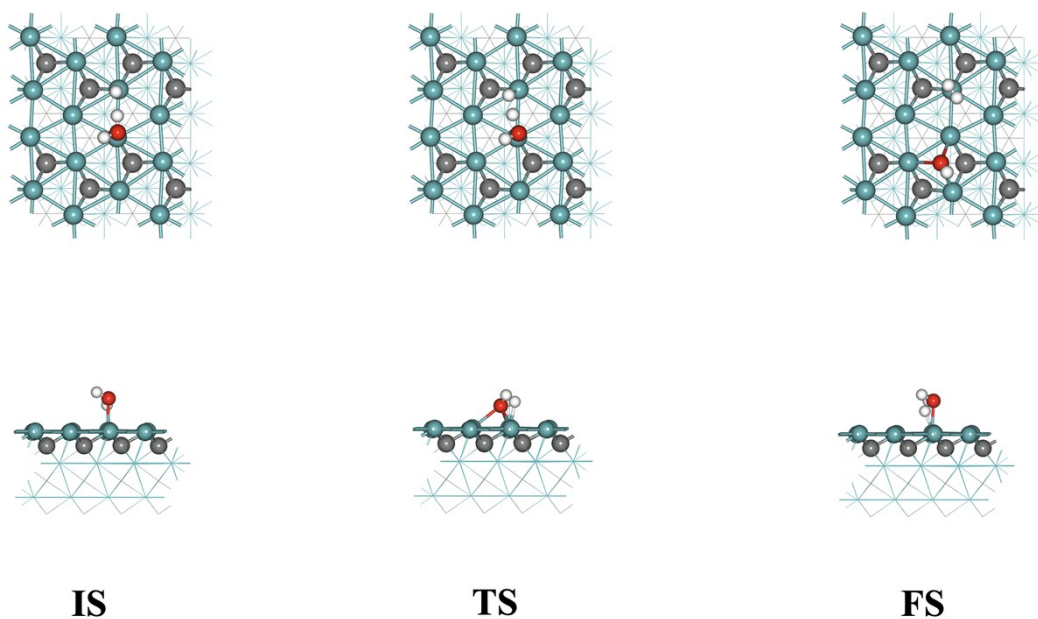
Figure S21. The mechanism of H$_2$ formation with a newly adsorbed H$_2$O on Mo$_2$C (200) from top and side view. The Mo, C, O, H atoms are respectively displayed in cyan, dark green, grey, red and white.
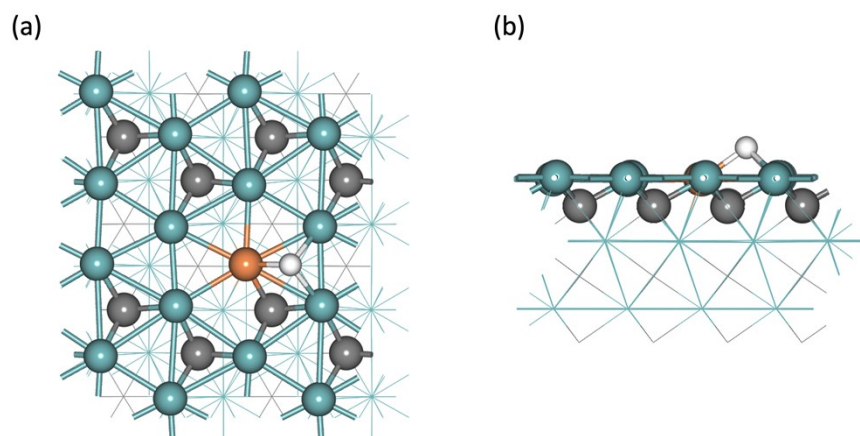
Figure S22. (a) and (b) The adsorption structure of H atom on the Ru$_1$-Mo$_2$C (200), from top and side view. The Ru, Mo, C, and H atoms are respectively displayed in orange, cyan, grey, and white.

a

$G_{ads} = -0.71$ eV

b

$G_{ads} = -0.69$ eV

c

$G_{ads} = -0.94$ eV

d

$G_{ads} = -0.52$ eV

Figure S23. Adsorption structures and the corresponding free adsorption energies of all reaction intermediates on Ru$_1$-Mo$_2$C(200).

a

$G_{ads} = -0.63$ eV

b

$G_{ads} = -0.94$ eV

c

$G_{ads} = -1.34$ eV

d

$G_{ads} = -0.68$ eV

Figure S24. Adsorption structures and the corresponding free adsorption energies of all reaction intermediates on $Mo_2C(200)$.

Table S1. Comparison of mass activity and turnover frequency (TOF) of recently reported noble metal-based HER catalysts in 1.0 M KOH electrolyte.

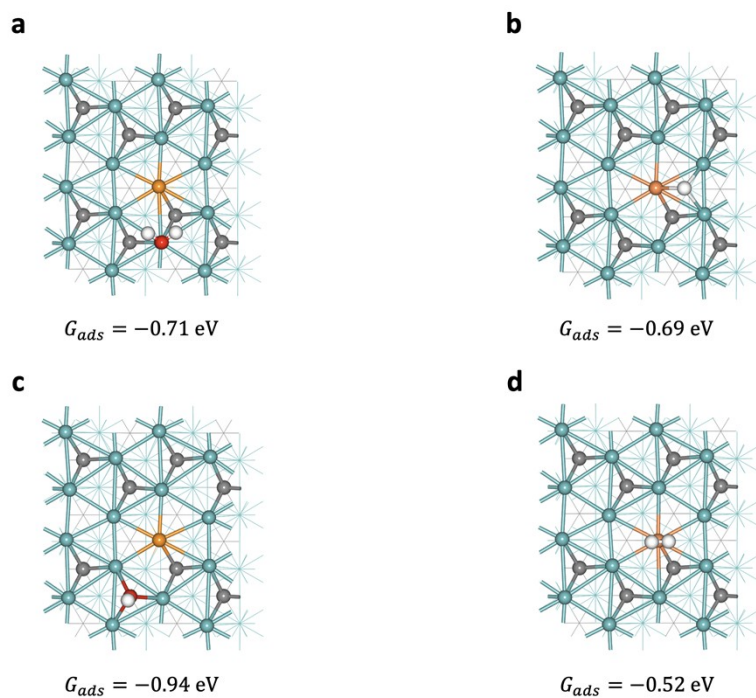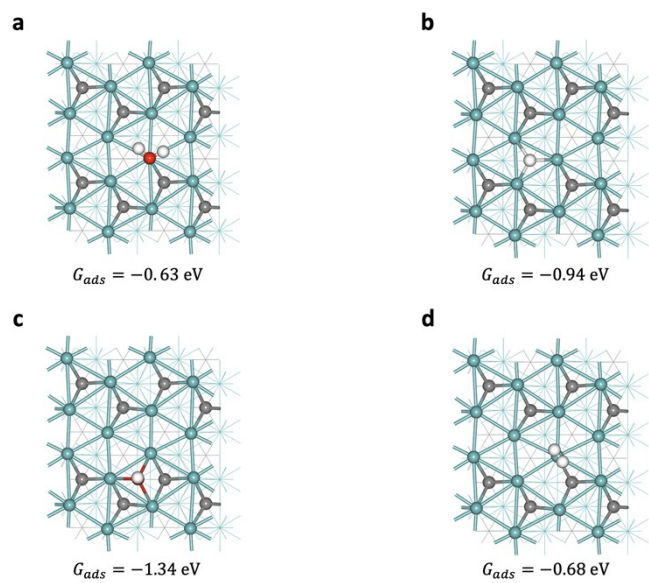| Electrocatalysts	Overpotential (V)	Mass activity (A/mg)	TOF (H$_2$ s^{-1})	References
Ru$_1$-Mo$_2$C NSs	**0.1**	**8.67**	**3.16**	**This work**
Au-Ru-2 NWs	0.05	/	0.31	*Nat. Chem.* **2018**
Ru@C$_2$N	0.05	/	1.66	*Nat. Nanotechnol.* **2017**
Ru$_{1,n}$-NC	0.025	1.7593	1.25	*Adv. Mater.* **2022**
Ru@Ni-MOF	0.05	~0.125	0.47	*Angew. Chem. Int. Ed.* **2021**
Ru/Co@OG	0.1		6.2	*Angew. Chem. Int. Ed.* **2021**
RuCo ANSs	0.1	/	8.52	*Angew. Chem. Int. Ed.* **2021**
Ru$_2$P/WO$_3$@NPC	0.07	~6	/	*Angew. Chem. Int. Ed.* **2021**
h-RuSe$_2$	0.05	/	0.34	*Angew. Chem. Int. Ed.* **2021**
Ru/OMSNNC	0.025	/	1.6	*Adv. Mater.* **2021**
Ru$_{\triangle c \to h}$/C	0.1	2.55	3.03/0.05	*Adv. Mater.* **2021**
R-NiRu	0.1	/	0.78	*Adv. Mater.* **2021**
Ru/NC-400	0.025	2/0.074	4.4	*Adv. Funct. Mater.* **2021**
RuCr@C	0.05	/	4.25	*Adv. Funct. Mater.* **2021**
S-RuP@NPSC-900	0.05	0.8715		*Adv. Sci.* **2020**
Ru/Fe-N-C	0.05	2.56	8.9	*Adv. Sci.* **2021**
Ru@GnP	0.025	0.23	~0.6	*Adv. Mater.* **2018**
Ru$_{SA+NP}$/DC	0.03	0.28	0.17	*Adv. Sci.* **2021**
2DPC-RuMo	0.05	/	3.57	*Adv. Mater.* **2020**
RuNi/CQDs-600	0.1	/	5.03	*Angew. Chem. Int. Ed.* **2020**
Ru@MWCNT	0.02	0.186	0.40/0.025	*Nat. Commun.* **2020**
Ru-MoO$_2$	0.1	/	0.53	*Adv. Energy Mater.* **2021**
Pt$_{doped}$@WCx	0.07	6.0	10.03/0.1	*Adv. Mater.* **2022**
Ru SAs-SnO$_2$/C	0.1	~3.3	5.44	*Angew. Chem. Int. Ed.* **2022**
Pt$_{SA}$/Mn$_3$O$_4$	0.05	0.374	10.11	*Energy Environ. Sci.* **2022**
Ru/Ni$_3$V-LDH	0.1	6.678	3.495	*J. Am. Chem. Soc.* **2022**
Pt/Pt$_5$P$_2$ PNCs	0.1	0.80	1.67/0.16	*Adv. Funct. Mater.* **2022**
RuP@RuP$_2$/C	0.02	0.1884	/	*Adv. Mater.* **2022**

Table S2. The comparison for HER performance of the state-of-the-art noble metal-based electrocatalysts in 1.0 M KOH electrolyte.

Electrocatalysts	Catalyst loading (mg cm^{-2})	Current density (mA cm^{-2})	Overpotential (mV)	References
Ru$_1$-Mo$_2$C NSs	**0.034**	**10**	**10.8**	**This work**
		100	**56.8**	
Au-Ru-2 NWs	0.08	10	50	*Nat. Chem.* **2018**
Ru@C$_2$N	0.285	10	17	*Nat. Nanotechnol.* **2017**
RuCo@NC	0.275	10	28	*Nat. Commun.* **2017**
Ru/Co$_{1.7}$@OG	0.214	10	24	*Angew. Chem. Int. Ed.* **2021**
Co-substituted Ru	0.153	10	13	*Nat. Commun.* **2018**
Ru@Ni-MOF	/	10	22	*Angew. Chem. Int. Ed.* **2021**
		100	112	
RuCo ANSs	/	10	10	*Angew. Chem. Int. Ed.* **2021**
		100	55	
Ru/OMSNNC	0.4	10	13	*Adv. Mater.* **2021**
RuP$_2$@NPC	1.0	10	52	*Angew. Chem. Int. Ed.* **2017**
Ru$_2$P/WO$_3$@NPC	~0.414	10	15	*Angew. Chem. Int. Ed.* **2021**
IrCo@NC-500	0.285	10	45	*Adv. Mater.* **2018**
RuCoP	0.3	10	23	*Energy Environ. Sci.* **2018**
		100	104	
Pt-Ni ASs	0.017(Pt)	10	27.7	*Adv. Mater.* **2018**
Pt$_3$Ni$_2$-NWs-S/C	0.015(Pt)	10	42	*Nat. Commun.* **2017**
Ru@GnP	0.25	10	22	*Adv. Mater.* **2018**
Ni@Ni$_2$P-Ru HNRs	/	10	31	*J. Am. Chem. Soc.* **2018**
Ru$_3$Ni$_3$ NAs	0.02(Ru)	10	39	*iScience* **2019**
Ru$_{SA+NP}$/DC	/	10	18.8	*Adv. Sci.* **2021**
2DPC-RuMo	0.324	10	18	*Adv. Mater.* **2020**
		100	83	
CoRu$_{0.5}$/CQDs	2	10	18	*Angew. Chem. Int. Ed.* **2021**
		100	225	
(Ru-Co)O$_x$	/	10	44.1	*Angew. Chem. Int. Ed.* **2020**
		100	89.1	
Ru-MoO$_2$	1.0	10	12	*Adv. Energy Mater.* **2021**
		100	200	
Pt$_{doped}$@WCx	0.25	10	20	*Adv. Mater.* **2022**
		100	58	
Ru SAs-SnO$_2$/C	~0.283	10	10	*Angew. Chem. Int. Ed.* **2022**
Pt$_{SA}$/Mn$_3$O$_4$	0.073(Pt)	10	24	*Energy Environ. Sci.* **2022**

		100	90	
Ru/Ni$_3$V-LDH	0.39	10	21	*J. Am. Chem. Soc.* **2022**
		100	~64	
Ru$_{1,n}$-NC	~0.142	10	14.8	*Adv. Mater.* **2022**
RuRh$_2$	~0.283	10	34	*Adv. Sci.* **2021**
R-NiRu	/	10	16	*Adv. Mater.* **2021**
		100	~82	
RuSi	0.562	10	19	*Angew. Chem. Int. Ed.* **2019**
h-RuSe$_2$	0.30	10	34	*Angew. Chem. Int. Ed.* **2021**
RhSe$_2$	/	10	81.6	*Adv. Mater.* **2021**
Ru/NC-400	0.2	10	39	*Adv. Funct. Mater.* **2021**
RuCr@C	~0.245	10	19	*Adv. Funct. Mater.* **2021**
		100	~63	
VRu$_{0.027}$O$_x$/GDY	0.286	10	13	*Adv. Sci.* **2021**
		100	75	
S-RuP@NPSC-900	/	10	92	*Adv. Sci.* **2020**
		100	~232	
Pt/Pt$_5$P$_2$ PNCs	~0.282	10	29	*Adv. Funct. Mater.* **2022**
		100	~148	
CoPt-Pt$_{SA}$/NDPCF	~0.281	10	31	*Adv. Funct. Mater.* **2022**
RuP@RuP$_2$/C	1	10	11.6	*Adv. Mater.* **2022**
Ru$_1$CoP/CDs-1000	0.42	10	51	*Angew. Chem. Int. Ed.* **2021**
		100	333	

Table S3. The comparison for AEMWE performance of Ru$_1$-Mo$_2$C catalysts with recent reports in 1.0 M KOH electrolyte.

Samples (PGM loading/mg cm^{-2})	Anodic catalysts	Activity	Operation time/h	References
Ru$_1$-Mo$_2$C (0.013)	**NiFe LDH**	**1. 83 V@1.0 A cm^{-2}**	**200@500 mA cm^{-2}**	**This work**
Pt/C (0.6)	NiCoFe-NDA	2.00 V@0.55 A cm^{-2}	100@325 mA cm^{-2}	*Energy Environ. Sci.* **2021**, *14*, 6546
Platinum black (3.0)	NiCoFeO$_x$	2.49 V@1.0 A cm^{-2}	3@200 mA cm^{-2}	*ACS Catal.* **2019**, *9*, 7
Pt/C (0.5)	NiFe-MOF	1.85 V@0.54 A cm^{-2}	72@460 mA cm^{-2}	*Energy Environ. Sci.* **2020**, *13*, 3447
Pt/C (0.94)	Fe$_x$Ni$_y$OOH-20F	1.80 V@1.0 A cm^{-2}	60@500 mA cm^{-2}	*ACS Catal.* **2020**, *11*, 264
Cl-Pt/LDH (0.01)	NiFe-LDH	1. 87 V@1.0 A cm^{-2}	20@1.0 A cm^{-2}	*Nat Commun* **2022**, *13*, 6875

Cl-Pt/LDH (0.01)	Ir/C	1. 99 V@1.0 A cm^{-2}	20@1.0 A cm^{-2}	
Pt$_1$/CoHPO (0.03)	Pt$_1$/CoHPO	1. 80 V@1.0 A cm^{-2}	100@400 mA cm^{-2}	*Nat Commun* **2022**, *13*, 3822
Pt@S-NiFe LDH	S-NiFe LDH	2.50 V@0.5 A cm^{-2}	200@500 mA cm^{-2}	*Adv. Mater.* **2023**, 2208209
Pt-AC/Cr−N−C (0.05)	NiFe-LDH	1. 90 V@1.0 A cm^{-2}	100@500 mA cm^{-2}	*J. Am. Chem. Soc.* **2023**, *145*, 21432
Pt/C (0.5)	IrO$_2$	1. 60 V@1.0 A cm^{-2}	1000@500 mA cm^{-2}	*Energy Environ. Sci.,* **2021**, *14*, 6338
Pt/C (0.2)	CoSb$_2$O$_6$	1. 90 V@0.8 A cm^{-2}	_	*ACS Energy Lett.* **2021**, *6*, 364
Pt-MoAl$_{1-x}$B (0.04)	RuO$_2$	2.00 V@1.0 A cm^{-2}	280@500 mA cm^{-2}	*Energy Environ. Sci.,* **2023**, *16*, 4093
Pt/C (-)	Ir@Zr–CoP	1.88 V@1.0 A cm^{-2}	150@500 mA cm^{-2}	*Adv. Energy Mater.* **2023**, *13*, 2301841
Pt/C (1.0)	NiFeV LDH	1.80 V@1.2 A cm^{-2}	100@500 mA cm^{-2}	*Small* **2021**, *17*, 2100639
Pt mesh	S-FeOOH	1.90 V@0.5 A cm^{-2}	24@1.0 A cm^{-2}	*Appl. Catal. B-environ.* **2022**, *315*, 121571
Pt/C (0.4)	IrO$_x$	1.80 V@1.15 A cm^{-2}	_	*Electrochim. Acta* **2019**, *295*, 99
Pt/C (0.4)	IrO$_2$	2.00 V@0.4 A cm^{-2}	100@400 mA cm^{-2}	*J. Membr. Sci.* **2019**, *581, 283*

Table S4. Free adsorption energies of H$_2$O on different sites of Ru$_1$-Mo$_2$C(200) surface. b-d are the Mo atoms corresponding to Figure S14.

Adsorption Site	Ru	Mo$_b$	Mo$_c$	Mo$_d$
G_a (eV)	-0.29	-0.63	-0.71	-0.60

Reference

(1)   Kresse, G.; Furthmüller, J. Efficient Iterative Schemes for Ab Initio Total-Energy Calculations Using a Plane-Wave Basis Set. *Phys. Rev. B - Condens. Matter Mater. Phys.* **1996**, *54*, 11169–11186.

(2)   Kresse, G.; Joubert, D. From Ultrasoft Pseudopotentials to the Projector Augmented-Wave Method. *Phys. Rev. B* **1999**, *59*, 1758–1775.

(3)   Perdew, J. P.; Burke, K.; Ernzerhof, M. Generalized Gradient Approximation Made Simple. *Phys. Rev. Lett.* **1996**, *77*, 3865–3868.

(4)   Grimme, S.; Ehrlich, S.; Goerigk, L. Effect of the Damping Function in Dispersion Corrected Density Functional Theory. *J. Comput. Chem.* **2011**, *32*, 1456–1465.

(5)   Blöchl, P. E.; Jepsen, O.; Andersen, O. K. Improved Tetrahedron Method for Brillouin-Zone Integrations. *Phys. Rev. B* **1994**, *49*, 16223–16233.

(6)   Pack, J. D.; Monkhorst, H. J. "special Points for Brillouin-Zone Integrations"-a Reply. *Phys. Rev. B* **1977**, *16*, 1748–1749.

(7)   Wang, H. F.; Liu, Z. P. Comprehensive Mechanism and Structure-Sensitivity of Ethanol Oxidation on Platinum: New Transition-State Searching Method for Resolving the Complex Reaction Network. *J. Am. Chem. Soc.* **2008**, *130*, 10996–11004.

(8)   Alavi, A.; Hu, P.; Deutsch, T.; Silvestrelli, P. L.; Hutter, J. CO Oxidation on Pt(111): An Ab Initio Density Functional Theory Study. *Phys. Rev. Lett.* **1998**, *80*, 3650–3653.

(9)   Michaelides, A.; Liu, Z. P.; Zhang, C. J.; Alavi, A.; King, D. A.; Hu, P. Identification of General Linear Relationships between Activation Energies and Enthalpy Changes for Dissociation Reactions at Surfaces. *J. Am. Chem. Soc.* **2003**, *125*, 3704–3705.

(10)   Liu, Z. P.; Hu, P. General Rules for Predicting Where a Catalytic Reaction Should Occur on Metal Surfaces: A Density Functional Theory Study of C-H and C-O Bond Breaking/Making on Flat, Stepped, and Kinked Metal Surfaces. *J. Am. Chem. Soc.* **2003**, *125*, 1958–1967.